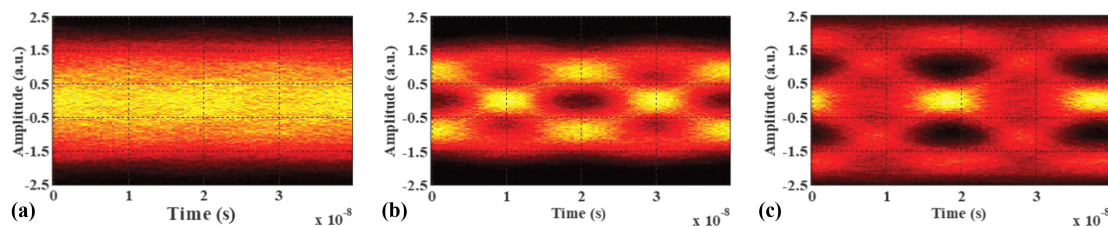


# Hartley-Domain DD-FTN Algorithm for ACO-SCFDM in Optical-Wireless Communications

Volume 11, Number 4, August 2019

Chun Shan  
Ji Zhou  
Dong Guo  
Haide Wang  
Long Liu  
Qi Wang  
Weiping Liu  
Changyuan Yu



DOI: 10.1109/JPHOT.2019.2925007

# Hartley-Domain DD-FTN Algorithm for ACO-SCFDM in Optical-Wireless Communications

Chun Shan,<sup>1</sup> Ji Zhou ,<sup>2</sup> Dong Guo ,<sup>3</sup> Haide Wang,<sup>2</sup> Long Liu,<sup>2</sup>  
Qi Wang ,<sup>4</sup> Weiping Liu,<sup>2</sup> and Changyuan Yu ,<sup>5</sup>

<sup>1</sup>School of Electronics and Information, Guangdong Polytechnic Normal University, Guangzhou 510665, China

<sup>2</sup>Department of Electronic Engineering, Jinan University, Guangzhou 510632, China

<sup>3</sup>School of Electronic Engineering, Beijing University of Posts and Telecommunications, Beijing 100876, China

<sup>4</sup>Huawei Technologies Co., Ltd., Shenzhen 518129, China

<sup>5</sup>Department of Electronic and Information Engineering, Hong Kong Polytechnic University, Hongkong

DOI:10.1109/JPHOT.2019.2925007

This work is licensed under a Creative Commons Attribution 3.0 License. For more information, see <https://creativecommons.org/licenses/by/3.0/>

Manuscript received May 27, 2019; revised June 18, 2019; accepted June 21, 2019. Date of publication June 26, 2019; date of current version July 16, 2019. This work was supported in part by the Local Innovation and Research Teams Project of Guangdong Pearl River Talents Program (2017BT01X121); in part by the Youth Science and Technology Innovation Talents of Guangdong (2015TQ01X606); in part by the Pearl River S&T Nova Program of Guangzhou (201710010051); in part by the Science and Technology Planning Project of Guangdong Province (2017B010123005); and in part by the Fundamental Research Funds for the Central Universities (21619309). Corresponding author: Ji Zhou (e-mail: zhouji@jnu.edu.cn).

**Abstract:** In this paper, we propose a Hartley-domain direct-detection faster-than-Nyquist (HD-DD-FTN) algorithm for asymmetrically clipped optical single-carrier frequency-division multiplexing (ACO-SCFDM) in optical-wireless communications (OWC). The HD-DD-FTN algorithm includes modified Hartley-domain equalization (HDE) and maximum likelihood sequence detection, which can simultaneously compensate serious high-frequency distortion and eliminate enhanced in-band noise for the bandwidth-limited OWC. Modified HDE can be implemented by real-valued operations, which is appropriate for dealing with real-valued signals. The simulation results show that ACO-SCFDM system using the HD-DD-FTN algorithm is more robust to inter-symbol interference than that using conventional HDE algorithm. Therefore, the bit error rate performance of the ACO-SCFDM system using HD-DD-FTN algorithm is better than that using the conventional HDE algorithm. In conclusion, the ACO-SCFDM system using the HD-DD-FTN algorithm shows great potential for bandwidth-limited OWC.

**Index Terms:** ACO-SCFDM system, HD-DD-FTN algorithm, optical-wireless communications, free-space communications.

## 1. Introduction

During recent decades, orthogonal frequency-division multiplexing (OFDM), which has advantages in terms of straightforward frequency-domain equalization (FDE) and resistance of inter-symbol interference (ISI), has remained a hot topic in areas of wireless and optical communications [1]–[5]. For intensity-modulated and direct-detection (IM/DD) optical-wireless communications (OWC), real-valued and non-negative OFDM systems are required, which have two common schemes of

DC-biased optical OFDM (DCO-OFDM) and asymmetrically clipped optical OFDM (ACO-OFDM) [6]–[8]. DCO-OFDM is generated by adding a moderate DC bias to bipolar real-valued OFDM signal. The DC bias reduces the clipping noise but inefficiently holds a large amount of optical power, which degrades the power efficiency. In the ACO-OFDM, only odd subcarriers are used to transmit data, making the negative part of the generated bipolar signals redundant. As a result, the non-negative ACO-OFDM signal is generated by clipping the negative part without losing any information. ACO-OFDM requires no DC bias, which has higher power efficiency than DCO-OFDM [9]–[11]. However, due to the nonuse of even subcarriers, the spectral efficiency of ACO-OFDM is worse. Layered ACO-OFDM has been proposed to improve the spectral efficiency [12]. In theory, when the number of layers increase, the spectral efficiency of layered ACO-OFDM gradually approaches that of DCO-OFDM [12]–[14]. Unfortunately, ACO-OFDM and layered ACO-OFDM inherits the high peak-to-average power ratio (PAPR) of OFDM, which is sensitive to nonlinearity in OWC. In our previous researches, we proposed the asymmetrically clipped optical single-carrier frequency-domain multiplexing (ACO-SCFDM) and layered ACO-SCFDM for IM/DD optical systems, which have lower PAPRs than conventional ACO-OFDM and layered ACO-OFDM, respectively [15], [16].

In OWC, the received optical signal is a combination of multipath light due to light reflections. The multipath effect gives rise to frequency-selective power fading, which seriously limits the effective bandwidth [17]–[19]. The longer the delay spread of the multipath, the smaller the effective bandwidth. Ref. [19] claims that, if an ACO-OFDM-based OWC system is deployed in a room where the delay spread of the channel is less than 16 ns, then the minimum 3-dB channel bandwidth is approximately 5 MHz. The limited bandwidth causes high-frequency distortion, which seriously degrades system performance. Therefore, transmitting more data on the limited bandwidth is an important issue in OWC. In ACO-SCFDM, channel equalization can effectively compensate the high-frequency fading distortions. However, in-band noise on high-frequency subcarriers is enhanced after channel equalization, leading to the increase of the bit error rate (BER). The direct-detection faster-than-Nyquist (DD-FTN) algorithm was proposed to simultaneously compensate the high-frequency fading distortions and eliminate enhanced in-band noise for bandwidth-limited optic-fiber communications [20]–[22].

In this paper, we first propose a Hartley-domain DD-FTN (HD-DD-FTN) algorithm for the ACO-SCFDM system in OWC. The HD-DD-FTN algorithm contains modified Hartley-domain equalization (HDE) and maximum likelihood sequence detection (MLSD). HDE is based on the real-valued Hartley transform, which is appropriate for dealing with real-valued signals [23]. Unlike the conventional HDE in our previous paper [24], the modified HDE owns both channel equalization and post filter functions. The channel equalization compensates the channel distortion, and the post filter eliminates the enhanced in-band noise but introduces a known ISI. Fortunately, the ISI can be eliminated by MLSD. After applying the modified HDE algorithm, MLSD can easily cancel the known ISI. Therefore, the proposed HD-DD-FTN algorithm can effectively compensate serious channel distortion and eliminate enhanced in-band noise at the same time. Finally, simulations are implemented to investigate the performance of ACO-SCFDM using the HD-DD-FTN algorithm for bandwidth-limited OWC.

The rest of this paper is organized as follows. In Section 2, the principles of the SCFDM encoder are demonstrated. The principles of HD-DD-FTN algorithm are given in Section 3. In Section 4, the simulation setups are described, and the simulation results of ACO-SCFDM using the HD-DD-FTN algorithm are presented and discussed. Finally, the paper is concluded in Section 5.

## 2. Principles of the SCFDM Encoder

In this section, the principles of anti-symmetrical SCFDM signal will be introduced. Fig. 1(a) shows the structure of the SCFDM encoder [15]. Before multiplexing, the generated  $M$ -PAM symbols are first sent to  $N$ -point discrete Hartley transform (DHT) to implement DHT-spread operation, which is

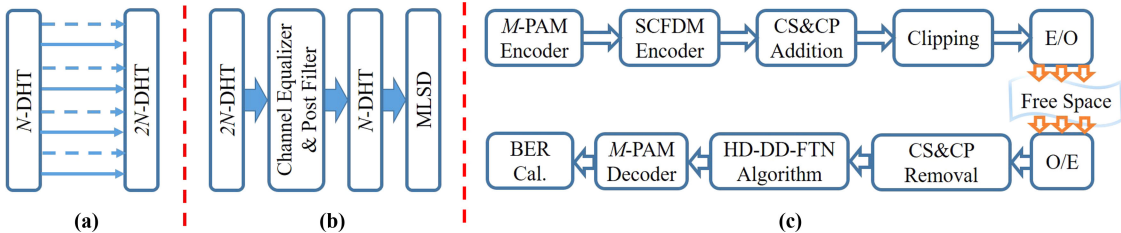


Fig. 1. (a) Structure of the SCFDM encoder; (b) Structure of the HD-DD-FTN algorithm; (c) Simulation setup of the ACO-SCFDM system using the HD-DD-FTN algorithm for OWC.

different from conventional OFDM. The output of  $N$ -point DHT is expressed as

$$Y(l) = \frac{1}{\sqrt{N}} \sum_{k=0}^{N-1} y(k) \text{cas}\left(\frac{2\pi lk}{N}\right), \quad l \in [0, N-1] \quad (1)$$

where  $\text{cas}(.) = \cos(.) + \sin(.)$ . Then, the output of  $N$ -point DHT is assigned to odd subcarriers of  $2N$ -point DHT for multiplexing,

$$\mathbf{X} = [0, Y(0), 0, Y(1), \dots, Y(N-1)]. \quad (2)$$

After  $2N$ -point DHT, the output is the generated SCFDM symbol, which can be expressed as

$$x(i) = \frac{1}{\sqrt{2N}} \sum_{h=0}^{2N-1} X(h) \text{cas}\left(\frac{2\pi hi}{2N}\right) = \frac{1}{\sqrt{2N}} \sum_{l=0}^{N-1} X(2l+1) \text{cas}\left(\frac{2\pi(2l+1)i}{2N}\right) \quad (3)$$

where  $i$  is from 0 to  $2N-1$ .

The expression of the generated SCFDM symbol can be further simplified. As shown in Eq. (2),  $X(2l+1)$  is equal to  $Y(l)$ . Therefore, the generated SCFDM symbol is rewritten as

$$x(i) = \frac{1}{\sqrt{2N}} \sum_{l=0}^{N-1} Y(l) \text{cas}\left(\frac{2\pi(2l+1)i}{2N}\right) = \frac{1}{\sqrt{2N}} \sum_{l=0}^{N-1} \sum_{k=0}^{N-1} y(k) \text{cas}\left(\frac{2\pi lk}{N}\right) \text{cas}\left(\frac{2\pi(2l+1)i}{2N}\right). \quad (4)$$

We can simplify the Eq. (4) to get the simplified expression of the generated SCFDM symbol,

$$x(i) = \begin{cases} [y(i)\cos(\frac{\pi i}{N}) + y(N-i)\sin(\frac{\pi i}{N})]/\sqrt{2}, & i \in [0, N-1]; \\ [y(i-N)\cos(\frac{\pi i}{N}) + y(2N-i)\sin(\frac{\pi i}{N})]/\sqrt{2}, & i \in [N, 2N-1]. \end{cases} \quad (5)$$

Since the SCFDM symbol generated by the proposed encoder is anti-symmetrical (i.e.,  $x(i) = -x(i+N)$ ), the ACO-SCFDM symbol can be obtained by clipping the negative part. As we know, the conventional OFDM symbol has high PAPR due to its Gaussian distribution. As Eq. (5) shows, the SCFDM symbols obey the distribution of the trigonometric function. Hence, the PAPR of the SCFDM symbol is lower than that of the conventional OFDM symbol. Moreover, based on Eq. (5), we designed a simplified SCFDM encoder to reduce the computational complexity from  $O(N \log_2 N)$  to  $O(N)$ [16].

### 3. Principles of the HD-DD-FTN Algorithm

In this section, we describe the principle of HD-DD-FTN algorithm in detail. The received signal is expressed as

$$\mathbf{z} = \mathbf{h} \otimes \mathbf{x} + \mathbf{w} \quad (6)$$

where  $\mathbf{h}$  is the channel impulse response,  $\mathbf{x}$  is the transmitted signal,  $\mathbf{w}$  is the additive white Gaussian noise (AWGN), and  $\otimes$  denotes the convolution operator. Fig. 1(b) shows the block diagram of the

HD-DD-FTN algorithm, which mainly includes a modified HDE and MLSD. First, a  $2N$ -point DHT is used to convert the time-domain received signal into a Hartley-domain signal, which is formulated as

$$\begin{aligned} Z(n) &= \frac{1}{\sqrt{2N}} \sum_{k=0}^{2N-1} (\mathbf{h} \otimes \mathbf{x} + \mathbf{w}) \text{cas} \left( \frac{2\pi nk}{2N} \right) \\ &= \begin{cases} H_e(n)X(n) + H_o(n)X(2N-n) + W(n), & n \in [1, 2N-1]; \\ H(0)X(0) + W(0), & n = 0 \end{cases} \end{aligned} \quad (7)$$

where

$$X(n) = \frac{1}{\sqrt{2N}} \sum_{k=0}^{2N-1} x(k) \text{cas} \left( \frac{2\pi nk}{2N} \right), \quad (8)$$

$$H(n) = \frac{1}{\sqrt{2N}} \sum_{k=0}^{2N-1} h(k) \text{cas} \left( \frac{2\pi nk}{2N} \right), \quad (9)$$

$$W(n) = \frac{1}{\sqrt{2N}} \sum_{k=0}^{2N-1} w(k) \text{cas} \left( \frac{2\pi nk}{2N} \right), \quad (10)$$

$$H_e(n) = [H(n) + H(2N-n)]/2, \text{ and} \quad (11)$$

$$H_o(n) = [H(n) - H(2N-n)]/2. \quad (12)$$

Depending on Eq. (7), conventional HDE is designed to remove channel distortion using the estimated channel matrixes  $H_e$  and  $H_o$ . After applying conventional HDE, the recovered signal can be expressed as

$$\begin{aligned} X(n) &= \frac{H_e(n)Z'(n) - H_o(n)Z'(2N-n)}{H_e(n)^2 + H_o(n)^2} \\ &= \begin{cases} Z'(n)/H_e^{\text{Ch}}(n) - Z'(2N-n)/H_o^{\text{Ch}}(n), & n \in [1, 2N-1]; \\ Z'(0)/H(0), & n = 0 \end{cases} \end{aligned} \quad (13)$$

where  $Z' = Z - W$ ,  $H_e^{\text{Ch}}(n) = [H_e(n)^2 + H_o(n)^2]/H_e(n)$ , and  $H_o^{\text{Ch}}(n) = [H_e(n)^2 + H_o(n)^2]/H_o(n)$ .

In ACO-SCFDM, only odd subcarriers are used to carrier data. After equalization, we extract the data  $X'$  from odd subcarriers. In other words,  $X'(l)$  is equal to  $X(2l+1)$  where  $l$  is from 0 to  $N-1$ . After  $N$ -point DHT, the  $\mathbf{x}'$  after equalization can be obtained. As shown in Eq. (13), the noise  $W(n)$  on the high-frequency subcarrier is enhanced after conventional HDE, which seriously degrades the performance of bandwidth-limited systems. The post filter can be used to eliminate the enhanced in-band noise. The output of the post filter is defined as

$$y(k) = \mathbf{h}^{\text{PF}} \otimes \mathbf{x}' = x'(k) + \alpha x'(k-1) \quad (14)$$

where  $\mathbf{h}^{\text{PF}}$  is the impulse response and  $\alpha$  is the coefficient of the post filter. The post filter can be also implemented in the Hartley domain, which is expressed as

$$Y(l) = \begin{cases} X'(l)H_e^{\text{PF}}(l) + X'(N-l)H_o^{\text{PF}}(l), & l \in [1, N-1]; \\ X'(0)H^{\text{PF}}(0), & l = 0 \end{cases} \quad (15)$$

where

$$H^{\text{PF}}(l) = \frac{1}{\sqrt{N}} \sum_{k=0}^{N-1} h^{\text{PF}}(k) \text{cas}\left(\frac{2\pi lk}{N}\right), \quad (16)$$

$$H_e^{\text{PF}}(l) = [H^{\text{PF}}(l) + H^{\text{PF}}(N-l)]/2, \quad (17)$$

$$H_o^{\text{PF}}(l) = [H^{\text{PF}}(l) - H^{\text{PF}}(N-l)]/2, \text{ and} \quad (18)$$

$$Y(l) = \frac{1}{\sqrt{N}} \sum_{k=0}^{N-1} y(k) \text{cas}\left(\frac{2\pi lk}{N}\right). \quad (19)$$

Therefore,  $Y(l)$  is simplified as

$$\begin{aligned} Y(l) &= \begin{cases} X(2l+1)H_e^{\text{PF}}(l) + X(2N-2l+1)H_o^{\text{PF}}(l) \\ X(1)H^{\text{PF}}(0) \end{cases} \\ &= \begin{cases} \begin{bmatrix} H_1(l) & H_2(l) & H_3(l) & H_4(l) \end{bmatrix} \begin{bmatrix} Z'(2l+1) \\ Z'(2N-2l-1) \\ Z'(2N-2l+1) \\ Z'(2l-1) \end{bmatrix}, & l \in [1, N-1]; \\ \begin{bmatrix} H^{\text{PF}}(0)/H_e^{\text{Ch}}(1) & -H^{\text{PF}}(0)/H_o^{\text{Ch}}(1) \end{bmatrix} \begin{bmatrix} Z'(1) \\ Z'(2N-1) \end{bmatrix}, & l=0 \end{cases} \end{aligned} \quad (20)$$

where

$$H_1(l) = H_e^{\text{PF}}(l)/H_e^{\text{Ch}}(2l+1), \quad (21)$$

$$H_2(l) = -H_e^{\text{PF}}(l)/H_o^{\text{Ch}}(2l+1), \quad (22)$$

$$H_3(l) = H_o^{\text{PF}}(l)/H_e^{\text{Ch}}(2l-1), \text{ and} \quad (23)$$

$$H_4(l) = H_o^{\text{PF}}(l)/H_o^{\text{Ch}}(2l-1). \quad (24)$$

Depending on Equations (20)–(24), we propose a modified HDE combining the conventional HDE with the Hartley-domain post filter. After applying the modified HDE, the enhanced in-band noise is effectively eliminated, but a known ISI as shown in Eq. (14) is introduced. Finally, MLSD is employed to cancel the ISI by minimizing squared Euclidean distance, expressed as

$$D = \sum_k \{y(k) - [t(k) + \alpha t(k-1)]\}^2. \quad (25)$$

MLSD employs the Viterbi algorithm to obtain the recovered signal  $t(k)$  from  $y(k)$ .

## 4. Simulation Setups and Results

In this section, numerical simulations are implemented by MATLAB to evaluate the performance of ACO-SCFDM using the HD-DD-FTN algorithm. We will introduce the simulation setups and investigate the simulation results.

### 4.1 Simulation Setups

Figure 1(c) depicts simulation setups of ACO-SCFDM using the HD-DD-FTN algorithm for OWC, and Table 1 shows the main parameters of the simulation setups. At the transmitter, the incoming binary bit sequence is mapped to the  $M$ -PAM signal. The mapped  $M$ -PAM signal is sent to the

TABLE 1

Main Parameters of Simulation Setups for the ACO-SCFDM System Using the HD-DD-FTN Algorithm

Parameters	Value
The modulation scheme	$M$ -PAM
Bandwidth	200 MHz
The number of total subcarriers	1024
The number of valid subcarriers	512
The length of CP & CS	64
The seed of bit sequence	21
The number of symbols	512
The number of training symbols	40
The number of samples per symbol	10
The pulse shaping	Rectangular
The channel model	Ceiling Bounce
The RMS delay spread	10 ns
The number of channel taps	30

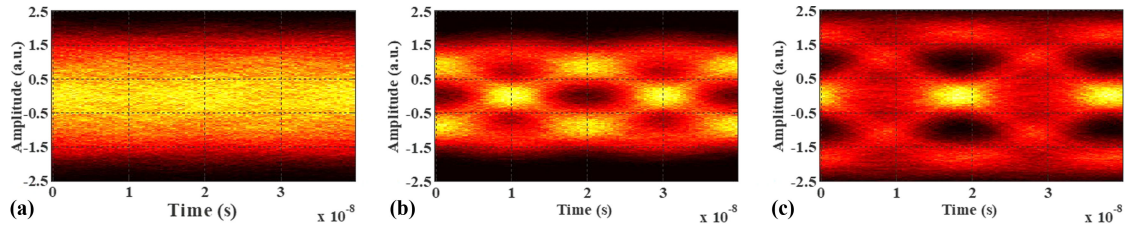


Fig. 2. (a) Eye diagram of the received signal before equalization; (b) Eye diagram of the recovered PAM-2 signal after conventional HDE; (c) Eye diagram of the signal after modified HDE in the HD-DD-FTN algorithm.

SCFDM encoder to generate the SCFDM signal. The simplified SCFDM encoder was proposed in our previous work [15]. After the addition of cyclic prefix (CP) and cyclic suffix (CS), the clipping operation is employed to remove the negative part of the bipolar SCFDM signals to generate ACO-SCFDM signals. Then, electro-optical (E/O) conversion is used to generate optical signals for transmission.

The generated optical signal is then propagated through the optical-wireless channel. The optical-wireless channel employs a free-space ceiling-bounce model in the simulations, which can model both multiple reflection light and single reflection light [17], [18]. In the simulations, the root-mean-square (RMS) delay spread is set as 10 ns and the corresponding 3-dB channel bandwidth is less than 8 MHz.

At the receiver, optical-electro (O/E) conversion converts the received optical signal to an electrical signal. After O/E conversion, the digital signal processing is implemented. First of all, the CP and CS are removed. Then, the proposed HD-DD-FTN algorithm is implemented to compensate the serious channel distortions and eliminate the enhanced in-band noise. Fig. 2(a) shows the eye diagram of the received signal before equalization. The channel distortions seriously degrade signal quality. Fig. 2(b) depicts the eye diagram of the recovered PAM-2 signal after the conventional HDE algorithm. The channel distortions are effectively compensated, but the in-band high-frequency noise is enhanced, resulting in the fuzzy eye diagram. Fig. 2(c) reveals the eye diagram of the signal after the modified HDE algorithm in the HD-DD-FTN algorithm. The signal after the modified HDE has distinct three-level amplitudes because that the enhanced in-band noise has been effectively eliminated and a known ISI is introduced after the modified HDE algorithm. The MLSD in the HD-

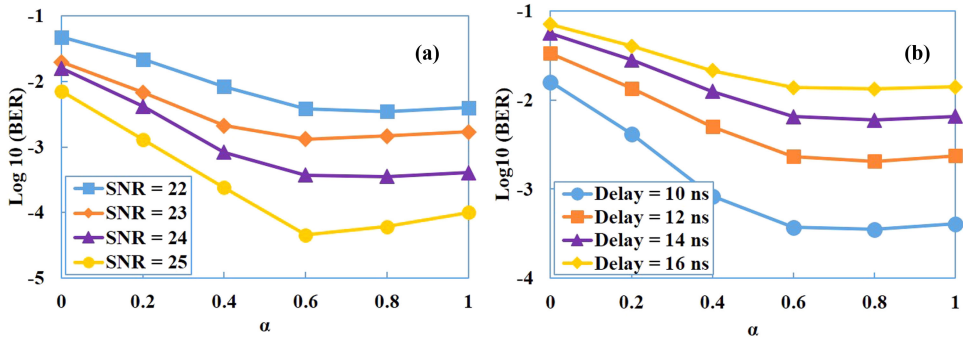


Fig. 3. BER versus  $\alpha$  of the HD-DD-FTN algorithm for the ACO-SCFDM system under (a) different SNRs and (b) different RMS delay spreads of the OWC channel.

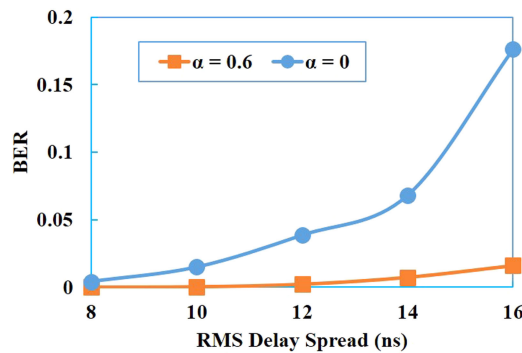


Fig. 4. BER versus the RMS delay spread of the OWC channel for ACO-SCFDM system using the HD-DD-FTN algorithm. When  $\alpha$  is set to 0, the HD-DD-FTN algorithm is equivalent to the conventional HDE algorithm.

DD-FTN algorithm can recover the  $M$ -PAM signal from the known ISI. Finally, the recovered  $M$ -PAM signal is decoded as a bit sequence for BER calculation.

#### 4.2 Simulation Results

Figure 3(a) shows BER versus  $\alpha$  of the HD-DD-FTN algorithm for the ACO-SCFDM system under different signal-to-noise ratios (SNRs). In ACO-SCFDM, 2-PAM is modulated, and data rate is set to 100 Mbit/s. The RMS delay spread is set to 10 ns. The curves show that BER decreases with the increase in  $\alpha$  at the beginning because the post filter in the HD-DD-FTN algorithm effectively eliminates the enhanced in-band noise. However, when  $\alpha$  is larger than 0.6, the BER performance begins to slightly deteriorate due to the increase in the residual ISI. MLSD in the HD-DD-FTN algorithm cannot completely handle the large known ISI. Fig. 3(b) depicts the BER versus  $\alpha$  of the HD-DD-FTN algorithm for the ACO-SCFDM system under different RMS delay spreads of the OWC channel. SNR is set to 24 dB. When  $\alpha$  is larger than 0.6, BER performance is not further improved under different RMS delay spreads. Therefore, in our simulations, the optimal  $\alpha$  is set to 0.6.

Figure 4 shows BER versus the RMS delay spread of the OWC channel for the ACO-SCFDM system. The RMS delay spread is set to a value from 8 ns to 16 ns. The SNR is set to 24 dB. As the principles of HD-DD-FTN algorithm in Section 3 reveal, the HD-DD-FTN algorithm is equivalent to the conventional HDE algorithm when  $\alpha$  is set to 0. Due to the narrower equivalent channel bandwidth, ISI increases with the increase of RMS delay spread. The BER performance of ACO-SCFDM degrades with increased ISI. Obviously, the ACO-SCFDM system with the HD-DD-FTN algorithm is more robust to ISI than that with conventional HDE algorithm.

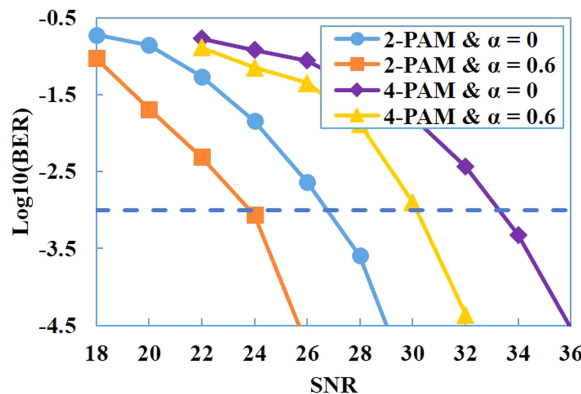


Fig. 5. BER against SNR for the 2-PAM and 4-PAM-modulated ACO-SCFDM systems using the HD-DD-FTN algorithm.

Figure 5 depicts BER against SNR for the 2-PAM and 4-PAM-modulated ACO-SCFDM systems using HD-DD-FTN algorithm. The RMS delay spread is set to 10 ns. The data rates of 2-PAM and 4-PAM-modulated ACO-SCFDM systems are 100 Mbit/s and 200 Mbit/s, respectively. When  $\alpha$  is set to 0.6, at a BER of  $10^{-3}$ , the required SNR for the 2-PAM-modulated ACO-SCFDM system using the HD-DD-FTN algorithm is approximately 3 dB less than that using conventional HDE algorithm. The required SNR for the 4-PAM-modulated ACO-SCFDM system using the HD-DD-FTN algorithm is approximately 3-dB less than that with the conventional HDE algorithm. The HD-DD-FTN algorithm has better performance than the conventional HDE algorithm.

## 5. Conclusions

In this paper, we propose the HD-DD-FTN algorithm to compensate the serious high-frequency distortion of the ACO-SCFDM system. The HD-DD-FTN algorithm can effectively compensate the serious channel distortion and eliminate the enhanced in-band noise at the same time. The simulation results show that the ACO-SCFDM system using the HD-DD-FTN algorithm is more robust to ISI than that using the conventional HDE algorithm. When RMS delay spread is set to 10 ns and  $\alpha$  is set to 0.6, at a BER of  $10^{-3}$ , the required SNR for the ACO-SCFDM system using the HD-DD-FTN algorithm is approximately 3 dB less than that using conventional HDE algorithm. In conclusion, the proposed ACO-SCFDM using the HD-DD-FTN algorithm presents great potential for OWC.

## References

- [1] J. Armstrong, "OFDM for optical communications," *J. Lightw. Technol.*, vol. 27, no. 3, pp. 189–204, Feb. 2009.
- [2] T. Mao, Z. Wang, Q. Wang, S. Chen, and L. Hanzo, "Dual-mode index modulation aided OFDM," *IEEE Access*, vol. 5, pp. 50–60, 2017.
- [3] H. Ye, G. Y. Li, and B. Juang, "Power of deep learning for channel estimation and signal detection in OFDM systems," *IEEE Wireless Commun. Lett.*, vol. 7, no. 1, pp. 114–117, Feb. 2018.
- [4] K. Mallick, R. Mukherjee, B. Das, G. C. Mandal, and A. S. Patr, "Bidirectional hybrid OFDM based Wireless-over-fiber transport system using reflective semiconductor amplifier and polarization multiplexing technique," *AEU Int. J. Electron. Commun.*, vol. 96, pp. 260–266, Nov. 2018.
- [5] K. Mallick, P. Mandal, G. C. Mandal, R. Mukherjee, B. Das, and A. S. Patr, "Hybrid MMW-over fiber/OFDM-FSO transmission system based on doublet lens scheme and POLMUX technique," *Opt. Fiber Technol.*, vol. 52, Nov. 2019, Art. no. 101942.
- [6] R. Mesleh, H. Elgala, and H. Haas, "On the performance of different OFDM based optical wireless communication systems," *J. Opt. Commun. Netw.*, vol. 3, no. 8, pp. 620–628, Aug. 2011.
- [7] J. Armstrong and A. J. Lowery, "Power efficient optical OFDM," *Electron. Lett.*, vol. 42, no. 6, pp. 370–372, Mar. 2006.
- [8] S. Dimitrov and H. Haas, "Information rate of OFDM-based optical wireless communication systems with nonlinear distortion," *J. Lightw. Technol.*, vol. 31, no. 6, pp. 918–929, Mar. 2013.

- [9] J. Armstrong and B. J. C. Schmidt, "Comparison of asymmetrically clipped optical OFDM and DC-biased optical OFDM in AWGN," *IEEE Commun. Lett.*, vol. 12, no. 66, pp. 343–345, May 2008.
- [10] S. D. Dissanayake and J. Armstrong, "Comparison of ACO-OFDM, DCO-OFDM and ADO-OFDM in IM/DD Systems," *J. Lightw. Technol.*, vol. 31, no. 7, pp. 1063–1072, Apr. 2013.
- [11] S. Dimitrov, S. Sinanovic, and H. Haas, "Clipping noise in OFDM-based optical wireless communication Systems," *IEEE Trans. Commun.*, vol. 60, no. 4, pp. 1072–1081, Apr. 2012.
- [12] Q. Wang, C. Qian, X. Guo, Z. Wang, D. G. Cunningham, and I. H. White, "Layered ACO-OFDM for intensity-modulated direct-detection optical wireless transmission," *Opt. Exp.*, vol. 23, no. 9, pp. 12382–12393, 2015.
- [13] A. J. Lowery, "Comparisons of spectrally-enhanced asymmetrically-clipped optical OFDM systems," *Opt. Exp.*, vol. 24, no. 4, pp. 3950–3966, 2016.
- [14] Q. Wang, Z. Wang, X. Guo, and L. Dai, "Improved receiver design for layered ACO-OFDM in optical wireless communications," *IEEE Photon. Technol. Lett.*, vol. 28, no. 3, pp. 319–322, Feb. 2016.
- [15] J. Zhou and Y. Qiao, "Low-PAPR asymmetrically clipped optical OFDM for intensity-modulation/direct-detection systems," *IEEE Photon. J.*, vol. 7, no. 3, Jun. 2015, Art no. 7101608.
- [16] J. Zhou *et al.*, "Low-PAPR layered/enhanced ACO-SCFDM for optical-wireless communications," *IEEE Photon. Technol. Lett.*, vol. 30, no. 2, pp. 165–168, Jan. 2018.
- [17] J. B. Carruthers and J. M. Kahn, "Modeling of nondirected wireless infrared channels," *IEEE Trans. Commun.*, vol. 45, no. 10, pp. 1260–1268, Oct. 1997.
- [18] J. M. Kahn and J. R. Barry, "Wireless infrared communications," *Proc. IEEE*, vol. 85, no. 2, pp. 265–298, Feb. 1997.
- [19] S. K. Wilson and J. Armstrong, "Transmitter and receiver methods for improving asymmetrically-clipped optical OFDM," *IEEE Trans. Wireless Commun.*, vol. 8, no. 9, pp. 4561–4567, Oct. 2009.
- [20] K. Zhong *et al.*, "140-Gb/s 20-km transmission of PAM-4 signal at 1.3  $\mu\text{m}$  for short reach communications," *IEEE Photon. Technol. Lett.*, vol. 27, no. 16, pp. 1757–1760, Aug. 2015.
- [21] K. Zhong, X. Zhou, J. Huo, C. Yu, C. Lu, and A. P. T. Lau, "Digital signal processing for short-reach optical communications: A review of current technologies and future trends," *J. Lightw. Technol.*, vol. 36, no. 2, pp. 377–400, Jan. 2018.
- [22] S. Liang, Z. Jiang, L. Qiao, X. Lu, and N. Chi, "Faster-than-Nyquist precoded CAP modulation visible light communication system based on nonlinear weighted look-up table predistortion," *IEEE Photon. J.*, vol. 10, no. 1, Feb. 2018, Art no. 7900709.
- [23] M. Svaluto Moreolo, R. Munoz, and G. Junyent, "Novel power efficient optical OFDM based on Hartley transform for intensity-modulated direct-detection systems," *J. Lightw. Technol.*, vol. 28, no. 5, pp. 798–805, Mar. 2010.
- [24] J. Zhou *et al.*, "Joint Hartley-domain and time-domain equalizer for a 200-G (4  $\times$  56-Gbit/s) optical PAM-4 system using 10G-class optics," *Opt. Exp.*, vol. 26, no. 26, pp. 34451–34460, Dec. 2018.